

Supporting information for:

**A computational study of direct CO₂ hydrogenation to methanol
on Pd catalysts**

Igor Kowalec ^a, Lara Kabalan ^a, C. Richard A. Catlow ^{a,b,c} and Andrew J. Logsdail ^{a,*}

^a Cardiff Catalysis Institute, School of Chemistry, Cardiff University, Cardiff, CF10 3AT, United Kingdom

^b UK Catalysis Hub, Research Complex at Harwell, RAL, Oxford, OX11 0FA, United Kingdom

^c Department of Chemistry, University College London, London, WC1H 0AJ, United Kingdom

* Email: LogsdailA@cardiff.ac.uk

S1. Bulk material

A primitive Pd unit cell with side length (a) of between 2.47 Å and 2.97 Å (corresponding to a cubic lattice parameter of 3.5 and 4.2 Å, respectively) was used to test and converge the Monkhorst-Pack \mathbf{k} -grid (reciprocal space sampling) and basis functions on the bulk energy (E_{bulk}). Convergence of the \mathbf{k} -grid within 10 meV was achieved with a (9 x 9 x 9) \mathbf{k} -grid, as shown in Figure S1, and computational time increased beyond that point without significant accuracy gain. Thus, a (9 x 9 x 9) \mathbf{k} -grid was determined to be the most suitable choice for further calculations on the Pd primitive cell, with \mathbf{k} -space sampling adjusted appropriately for models with larger supercells (i.e. slabs).

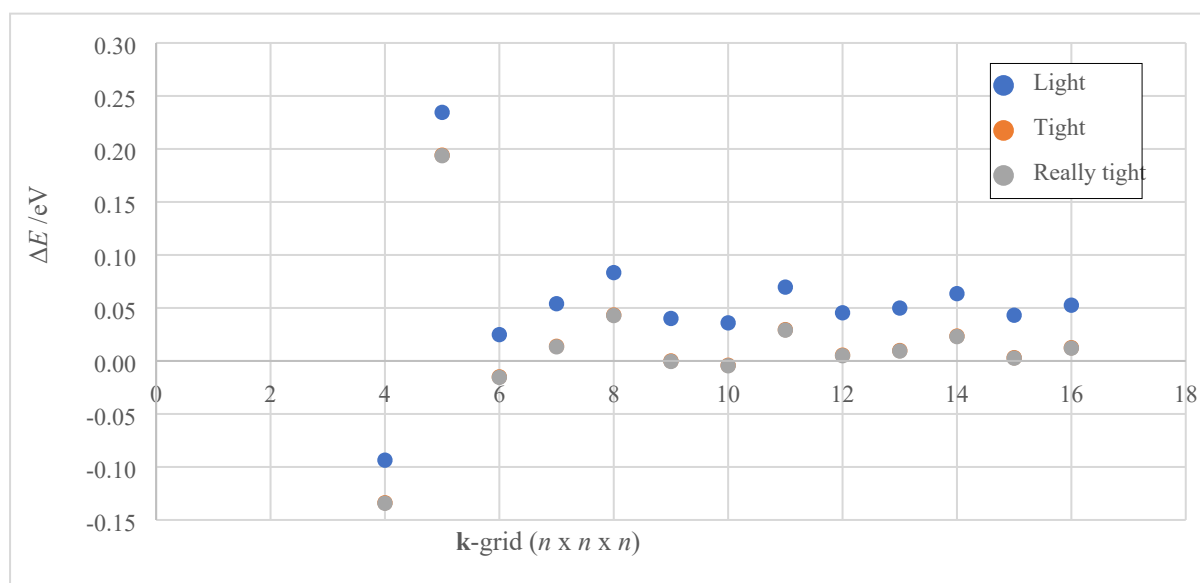


Figure S1. Convergence of energy with respect to \mathbf{k} -grid and basis set choice, sampled on a Pd primitive cell with a unit cell vector of 2.69 Å, where n corresponds to the \mathbf{k} -grid sampling. The energy difference (ΔE) is presented relative to that calculated with a “tight” basis set and a (9 x 9 x 9) \mathbf{k} -grid.

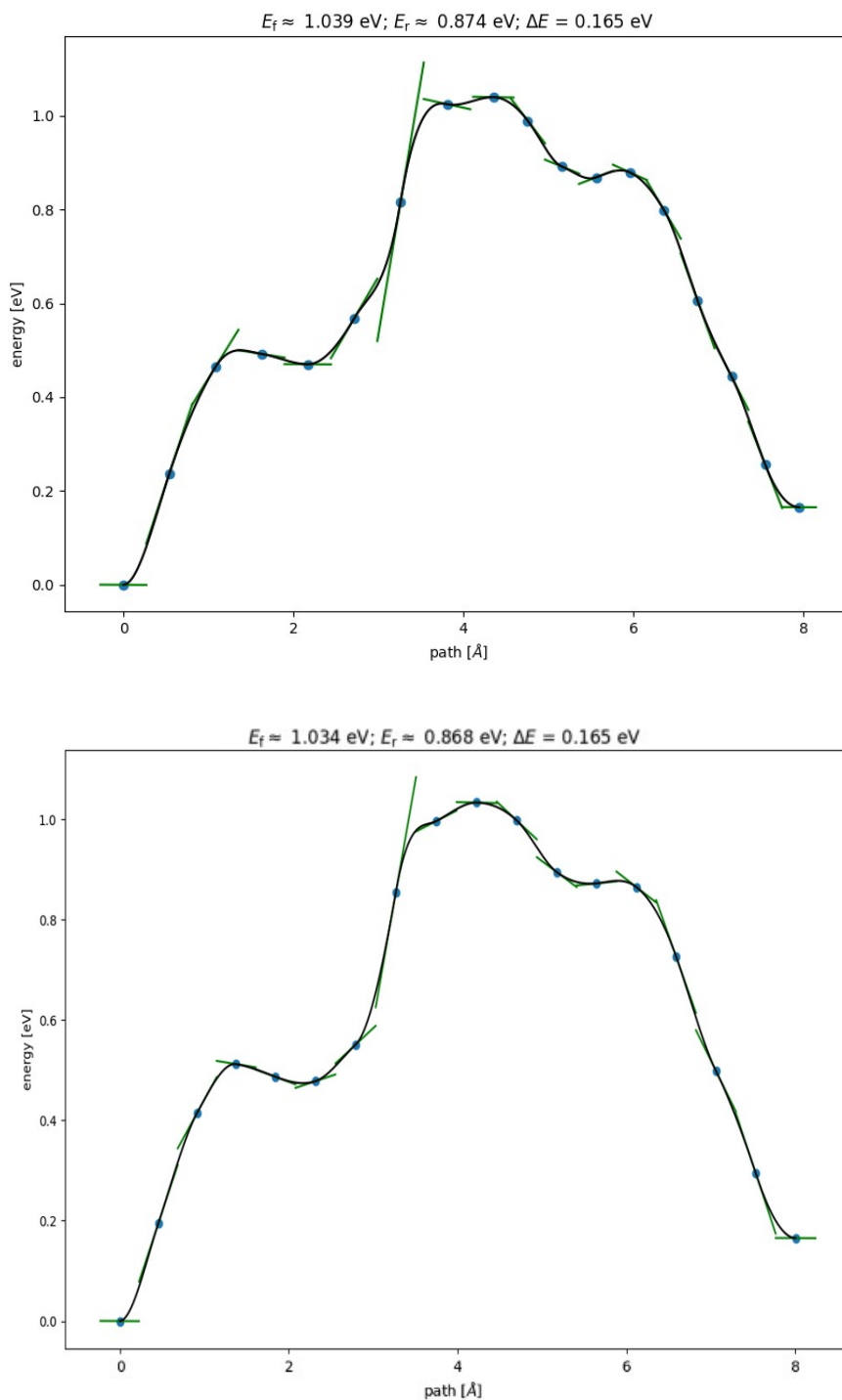
The standard basis sets that are distributed with the FHI-aims package were used, categorized as “light”, “tight” and “very tight”. A significant gain in energetic accuracy was observed when changing from the “light” to the “tight” settings; however, the calculations were twice as expensive. The “very tight” basis only marginally improved energetic accuracy, by on average 0.5 meV with respect to the “tight” settings; this increase in computational cost with little accuracy gain made further consideration of this setting inappropriate.

Using the outlined \mathbf{k} -grid and basis set choices, a_0 and the bulk modulus, B_0 , was calculated using the Birch-Murnaghan equation of state, with a range of common exchange-correlation (XC) functionals considered, and the results are shown in Table S1.¹ Selection of an appropriate exchange-correlation density functional was made based on accuracy, and computational time required for a single-point calculation. The PW-LDA XC functional underestimates the Pd bulk a_0 and overestimates B ; The PBE XC functional is inaccurate also, but introduction of a Van der Waals correction, represented using the

Tkatchenko-Scheffler method, yields values of $a_0 = 3.914 \text{ \AA}$ and $B_0 = 183.8 \text{ GPa}$, with only a small error of +0.9 % and +1.8 % with respect to experiment.^{2,3} Furthermore, the cohesive energy (E_{coh}) of 4.00 eV agrees reasonably with literature.^{4,5} Therefore, the generalized gradient approximation (GGA) based on the Perdew-Burke-Ernzerhof exchange-correlation functional, with a Tkatchenko-Scheffler van der Waals correction (PBE+vdW), was used for all subsequent calculations.⁶

Table S1. Screening of exchange correlation functionals with respect to accuracy for a_0 (\AA), B_0 (GPa) and E_{coh} (eV), as acquired using a Birch-Murnaghan Equation of State, and the difference in each property with respect to experiment (Δ , given in %). PBE+MBD includes the many-body dispersion (MBD) correction of Tkatchenko *et al.*^{7,8}

Settings	Basis	a_0	Δa_0	B_0	ΔB_0	E_{coh}	ΔE_{coh}
Exp. ² (293.15 K)	-	3.890	-	-	-	3.89	-
Exp. ³ (0 K)	-	3.878	-	180.40	-	-	-
PW-LDA	Light	3.841	-1.0 %	226.13	20.2 %	5.08	30.6%
PBE	Light	3.944	1.7 %	168.60	-7.0 %	3.73	-4.1%
PBE+TS	Light	3.914	0.9 %	183.77	1.8 %	4.00	2.7 %
PBE+TS	Tight	3.910	0.8 %	186.39	3.2 %	4.01	3.0 %
PBE+MBD	Light	3.920	1.1 %	179.59	-0.4 %	4.05	4.1%
B3LYP	Light	3.989	2.9 %	140.19	-28.7 %	2.50	-35.7 %



S2. Transition state search convergence criteria comparison

Figure S2. Energy profile of the initial CO_2 hydrogenation step on the Pd (111) surface, as calculated using the MLNEB approach. Top: Results with $f_{\text{max}} = 0.05 \text{ eV/\AA}$, fit uncertainty = 0.03; Bottom: $f_{\text{max}} = 0.01 \text{ eV/\AA}$ and fit uncertainty = 0.05.

S3. Effect of spin treatment on E_{act}

Table S2. Comparison of E_{act} when using spin-paired or spin-collinear approximations, with impact considered across all intermediate steps in the CO₂ hydrogenation reaction over the FCC Pd (111), (110) and (100) surfaces. Species given in the Table are those at the start of the reaction step. All energies are in eV.

Pd Surface	Species	E_{act} (spin-paired)	E_{act} (spin-collinear)	ΔE_{act}
(100)	CO ₂ ^{δ-}	1.07	1.08	-0.01
	HCOO	0.74	0.70	0.04
	HCOOH	1.26	1.29	-0.04
	H ₂ COOH	0.80	0.77	0.03
	H ₂ CO	0.63	0.63	0.00
	H ₃ CO	0.70	0.69	0.01
(110)	CO ₂ ^{δ-}	0.83	0.82	0.02
	HCOO	0.65	0.62	0.03
	HCOOH	0.92	0.96	-0.05
	H ₂ COOH	0.52	0.49	0.02
	H ₂ CO	0.65	0.64	0.01
	H ₃ CO	0.40	0.39	0.01
(111)	CO ₂ ^{δ-}	1.09	1.05	0.03
	HCOO	0.57	0.54	0.03
	HCOOH	1.35	1.34	0.01
	H ₂ COOH	0.50	0.51	0.00
	H ₂ CO	0.77	0.75	0.01
	H ₃ CO	0.49	0.48	0.01

S4. Tabulated adsorption enthalpy and energy

Table S3 The adsorption energy, E_{ads} , and the adsorption enthalpy, H_{ads} , across all intermediates in the CO_2 hydrogenation reaction over the FCC Pd (111), (110) and (100) surfaces. All numerical values are in eV.

Adsorbate	$H_{\text{ads}} / \text{eV}$			$E_{\text{ads}} / \text{eV}$		
	Pd (111)	Pd (100)	Pd (110)	Pd (111)	Pd (100)	Pd (110)
CO_2	-0.21	-0.18	-0.16	-0.21	-0.18	-0.16
$\text{CO}_2^{\delta-}$	0.09	-0.09	-0.19	0.06	-0.13	-0.23
HCOO	-2.46	-2.55	-2.72	-2.65	-2.73	-2.90
HCOOH	-0.63	-0.64	-0.50	-0.67	-0.67	-0.54
H_2COOH	-1.93	-2.12	-2.25	-2.11	-2.35	-2.40
CH_2O	-0.58	-0.83	-0.94	-0.75	-0.93	-1.05
CH_3O	-2.33	-2.51	-2.39	-2.13	-2.35	-2.17
CH_3OH	-0.52	-0.52	-0.66	-0.58	-0.57	-0.71

S5. Tabulated energy of individual reaction steps

Table S4. The reaction energy (eV) of intermediate steps in CO₂ hydrogenation on the Pd (111), (110), and (100) surfaces. Each calculation is balanced stoichiometrically with energies of gas-phase molecules. * represents the catalyst surface.

Reaction step	Pd (111)	Pd (110)	Pd (100)	Pd (111) + ZPE	Pd (110) + ZPE	Pd (100) + ZPE
* + CO ₂ + 3 H ₂	0.00	0.00	0.00	0.00	0.00	0.00
*CO ₂ ^{δ-} + 3 H ₂	0.06	-0.23	-0.13	0.09	-0.19	-0.09
CO ₂ ^{δ-} + H + 2.5 H ₂	-0.59	-0.67	-0.67	-0.53	-0.49	-0.61
TS1 + 2.5 H ₂	0.49	0.17	0.40	0.60	0.33	0.49
HCOO* + 2.5 H ₂	-0.37	-0.62	-0.45	-0.15	-0.37	-0.24
HCOO* + H* + 2 H ₂	-0.81	-1.02	-0.99	-0.57	-0.74	-0.77
TS2 + 2 H ₂	-0.24	-0.37	-0.25	-0.06	-0.19	-0.10
HCOOH* + 2 H ₂	-0.75	-0.61	-0.74	-0.40	-0.20	-0.41
HCOOH* + H* + 1.5 H ₂	-1.37	-1.14	-1.32	-0.99	-0.59	-1.06
TS3 + 1.5 H ₂	-0.02	-0.23	-0.07	0.42	0.25	0.45
H ₂ COOH* + 1.5 H ₂	-0.11	-0.49	-0.32	0.38	0.15	0.09
TS4 + 1.5 H ₂	0.36	0.03	0.37	0.78	0.59	0.77
H ₂ CO* + OH* + 1.5 H ₂	0.29	-0.42	-0.38	0.71	0.13	0.06
H ₂ CO* + H ₂ O* + H ₂	-0.93	-1.28	-1.10	-0.37	-0.58	-0.55
H ₂ CO* + H ₂ O + H ₂	-0.52	-0.82	-0.70	-0.02	-0.19	-0.21
H ₂ CO* + H* + H ₂ O + 0.5 H ₂	-1.00	-1.17	-1.23	-0.47	-0.52	-0.77
TS5 + H ₂ O + 0.5 H ₂	-0.23	-0.52	-0.60	0.27	0.14	-0.08
H ₃ CO* + H ₂ O + 0.5 H ₂	-0.51	-0.81	-0.99	0.14	-0.03	-0.29
H ₃ CO* + H* + H ₂ O	-1.15	-1.25	-1.57	-0.47	-0.50	-0.94
TS6 + H ₂ O	-0.66	-0.86	-0.87	-0.02	-0.08	-0.21
H ₃ COH* + H ₂ O	-1.62	-1.76	-1.54	-0.75	-0.75	-0.68
* + CH ₃ OH + H ₂ O	-1.05	-1.05	-1.05	-0.26	-0.26	-0.26

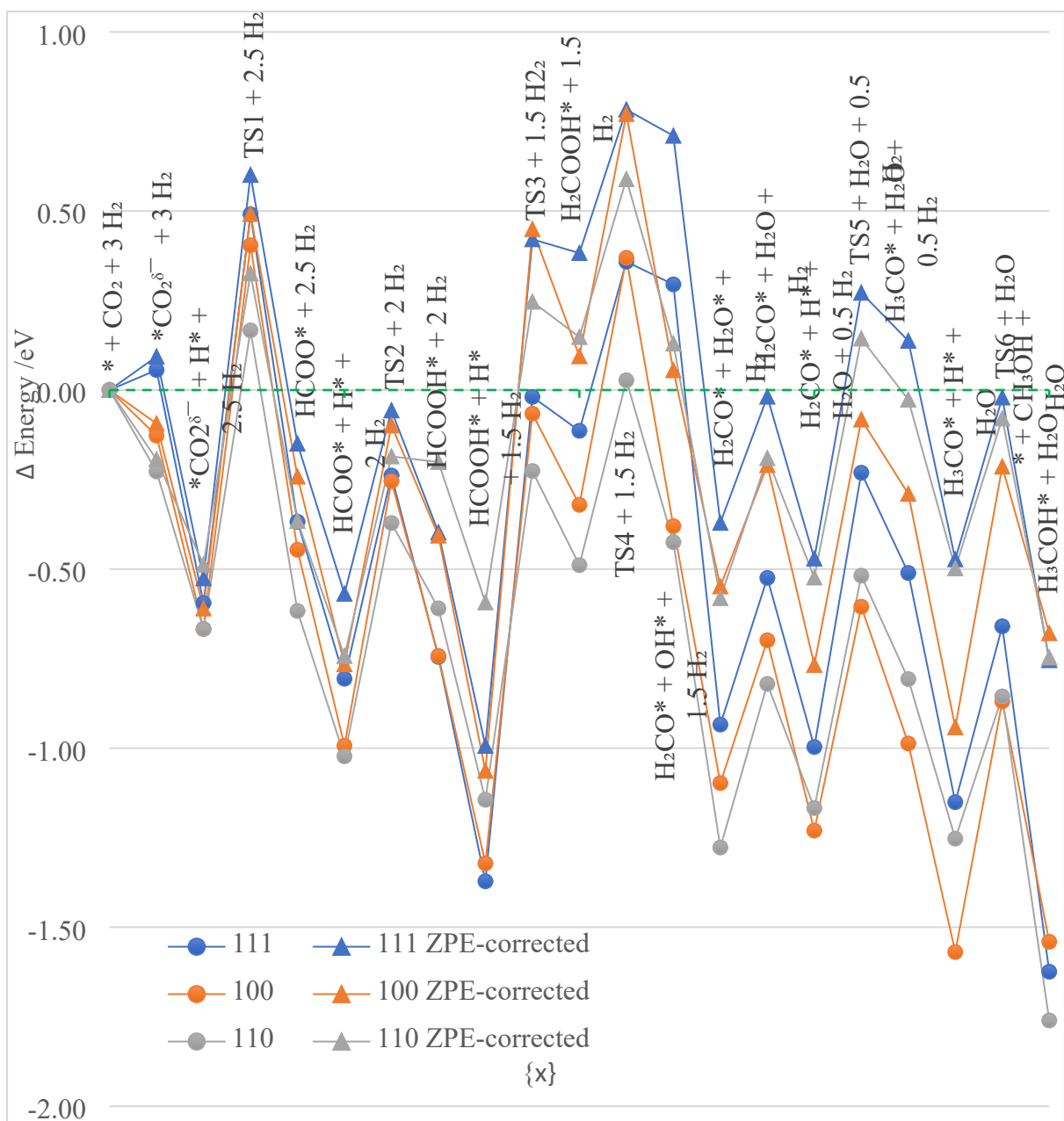
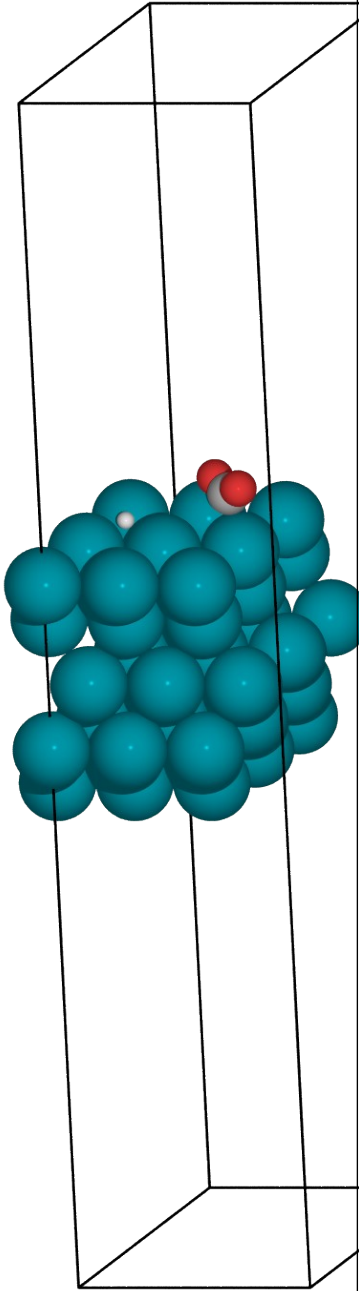
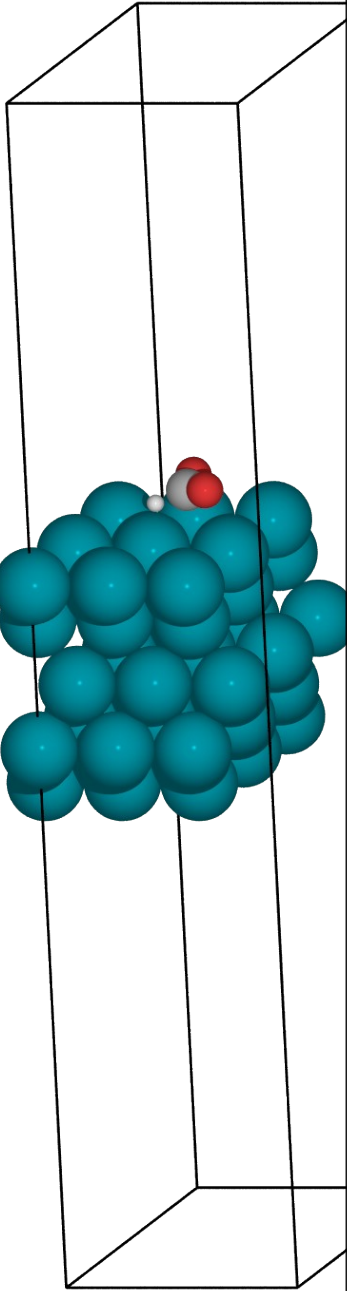
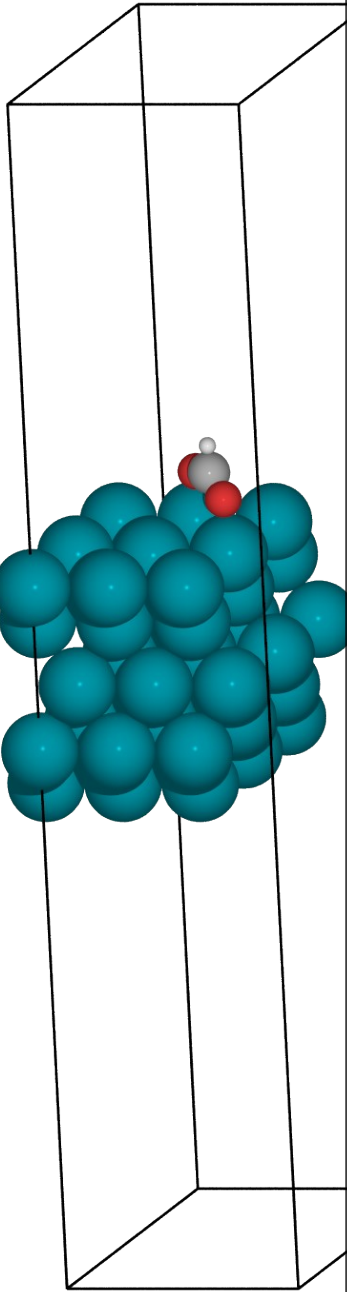
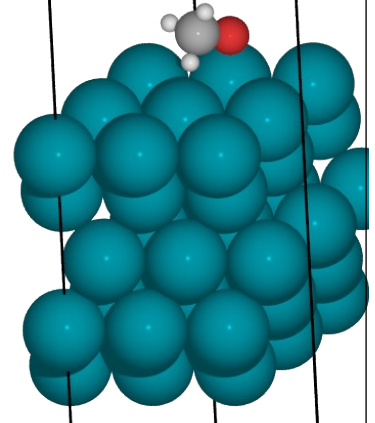
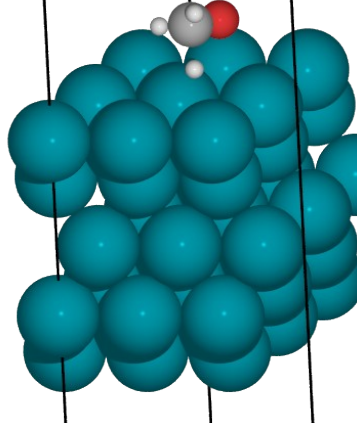
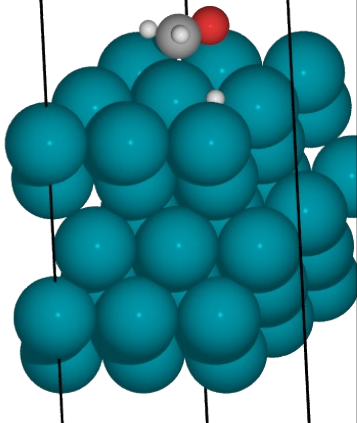
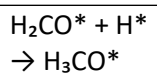
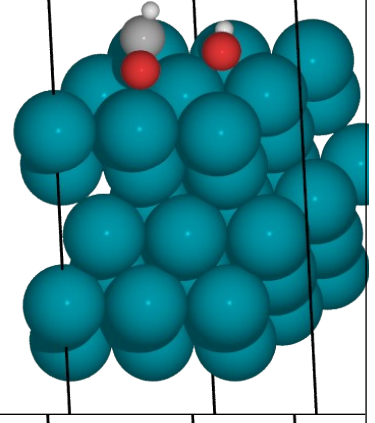
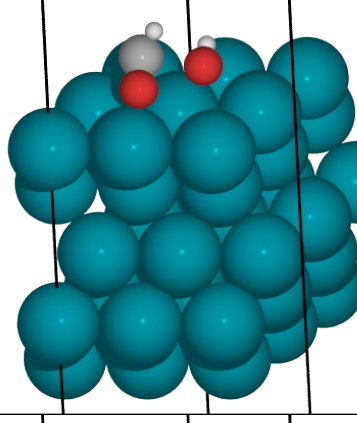
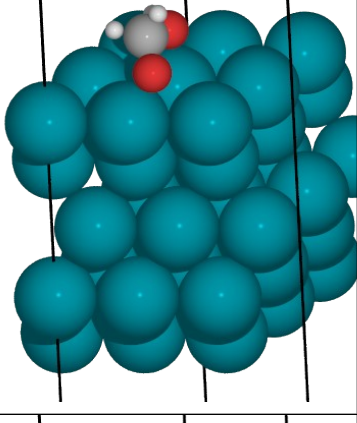
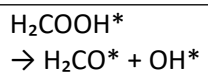
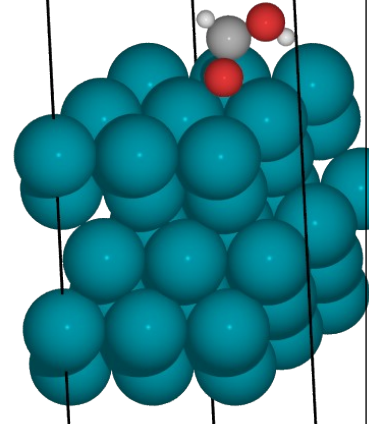
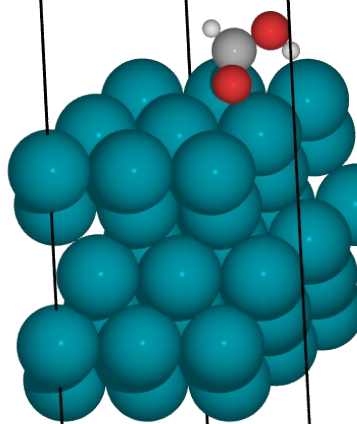
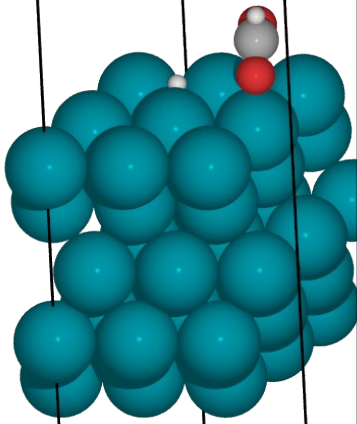
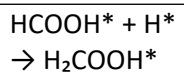
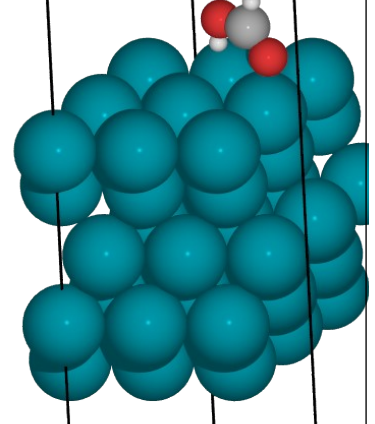
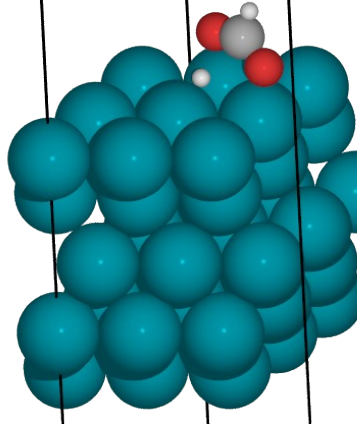
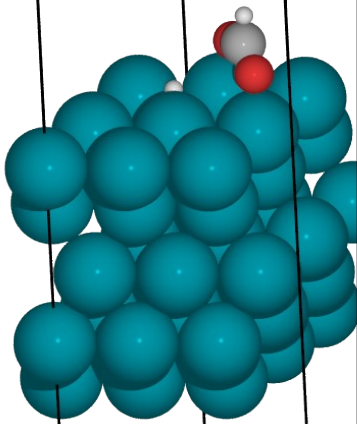
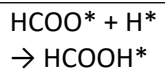


Figure S3. The energy profile of CO₂ hydrogenation to methanol, *via* the formate pathway, on Pd (111), (100), and (110) surfaces with and without ZPE-correction included, plotted in blue, orange, and grey, respectively, relative to the energy of pristine surface and gas phase reactants.²⁵ Energies of intermediate structures and transition state geometries have been stoichiometrically balanced with energies of gas phase reactants; * indicates surface bound species.

S6. Visualised adsorbates and transition states

Table S5. Graphical representation of initial, transition state and final geometries in E_{act} calculations on Pd (111) surface. The blue, red, grey and white spheres represent Pd, O, C and H atoms; the black lines indicate the edges of the simulation cell. The full size of the simulation cell, including all unit cell borders, is depicted for the initial reaction step to illustrate the vacuum region size.

Reaction	Initial geometry	Transition state geometry	Final geometry
$^*\text{CO}_2^{\delta-} + \text{H}^* \rightarrow \text{HCOO}^*$			



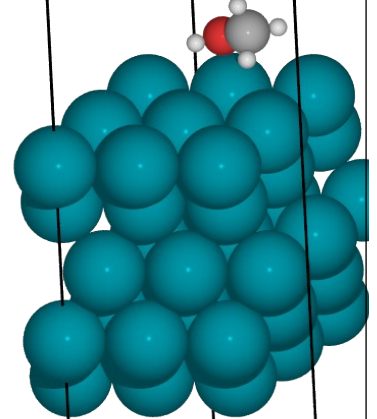
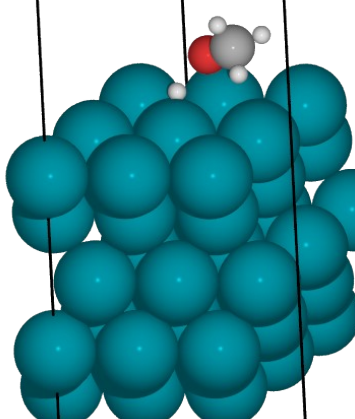
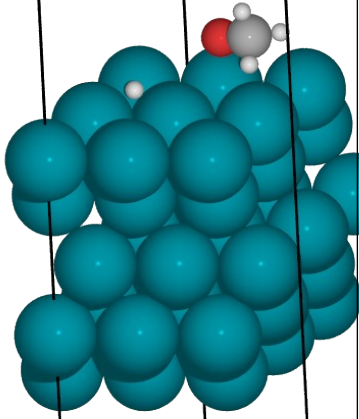
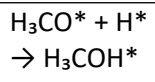
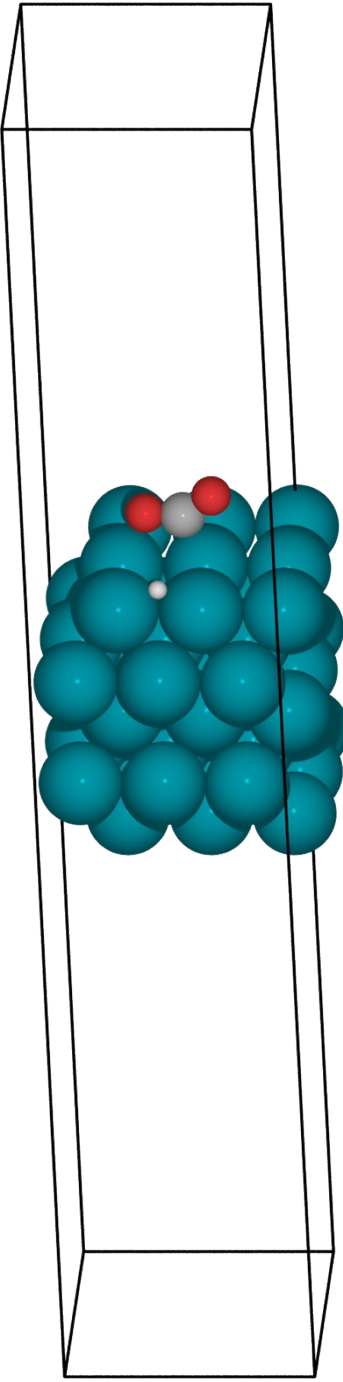
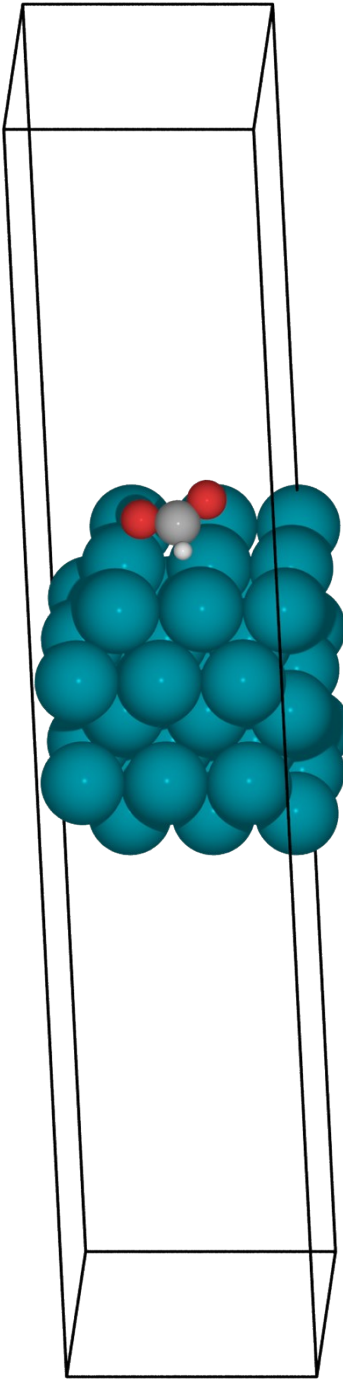
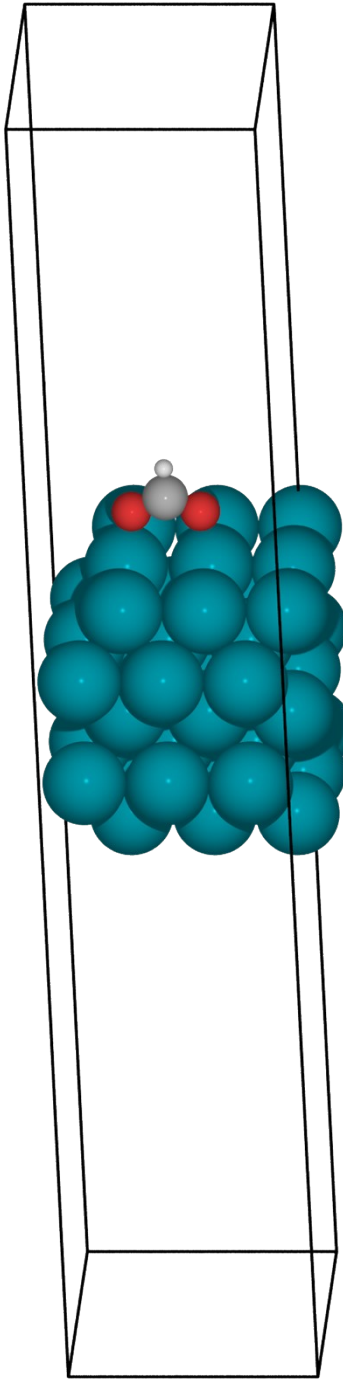
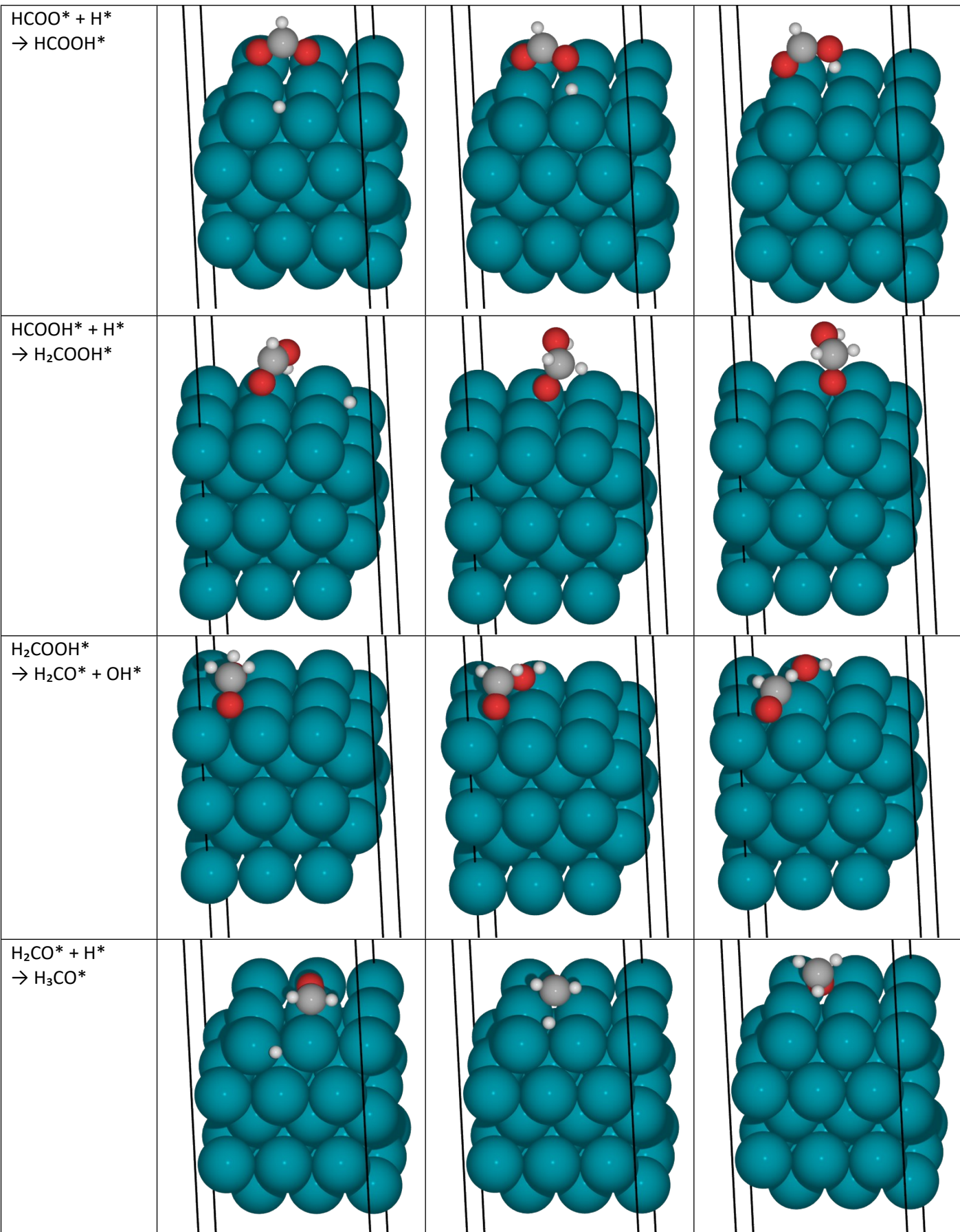


Table S6. Graphical representation of initial, transition state and final geometries in E_{act} calculations on Pd (100) surface. The blue, red, grey and white spheres represent Pd, O, C and H atoms; the black lines indicate the edges of the simulation cell. The full size of the simulation cell, including all unit cell borders, is depicted for the initial reaction step to illustrate the vacuum region size.

Reaction	Initial geometry	Transition state geometry	Final geometry
$\text{*CO}_2^{\delta-} + \text{H*}$ $\rightarrow \text{HCOO*}$			



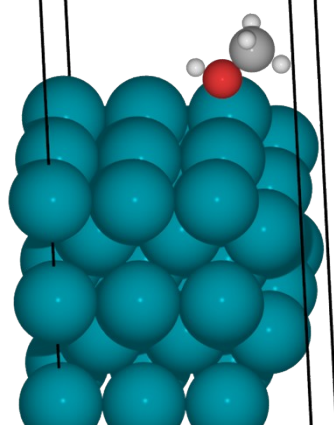
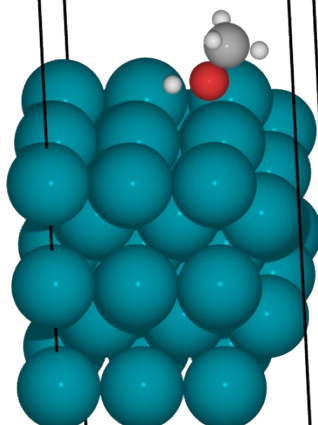
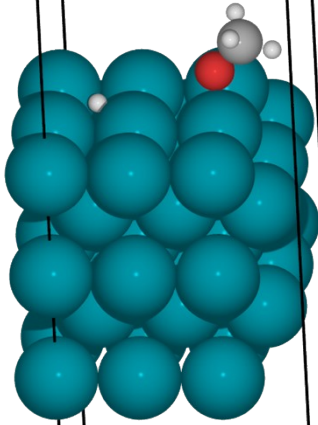
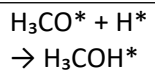
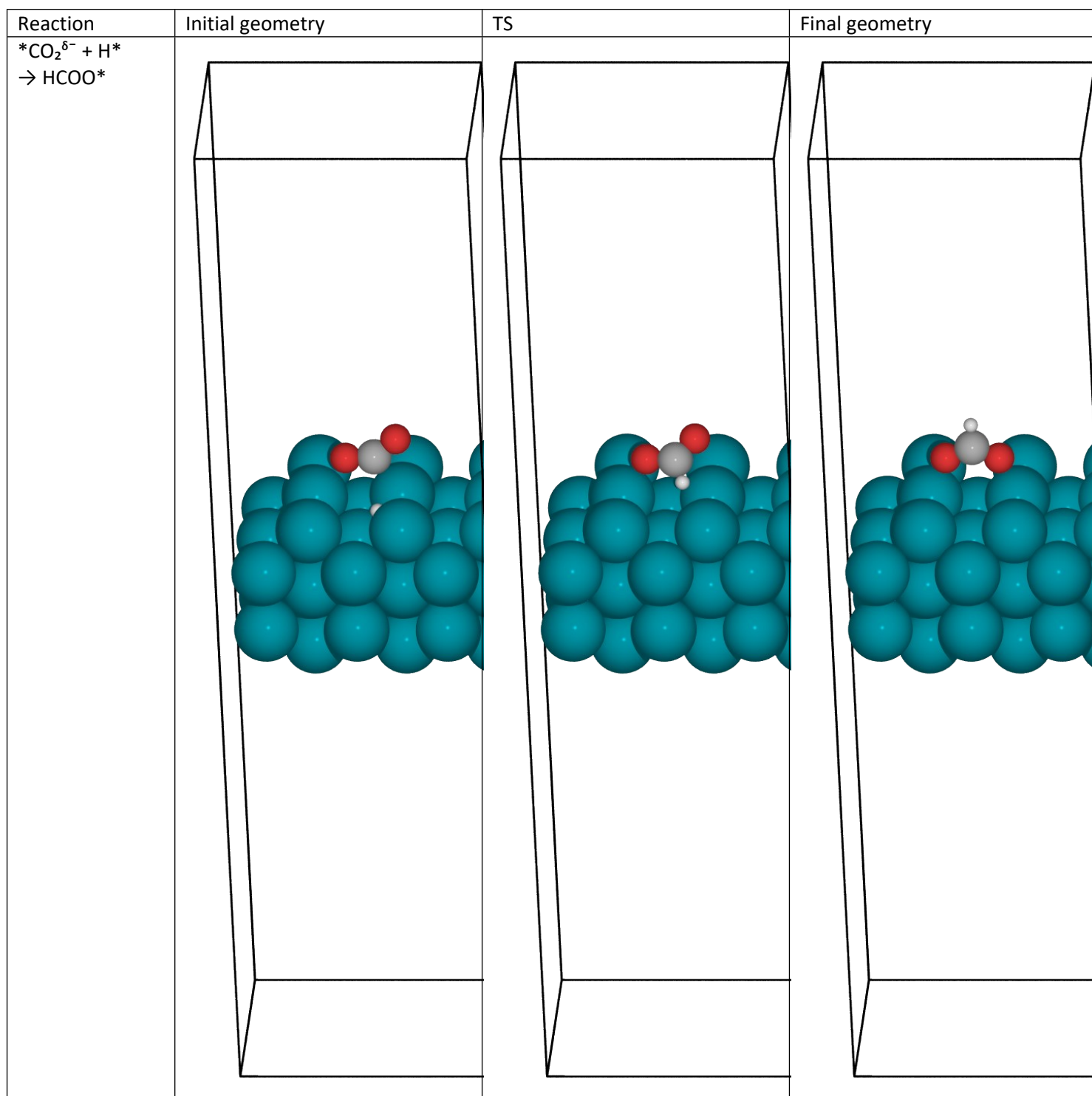
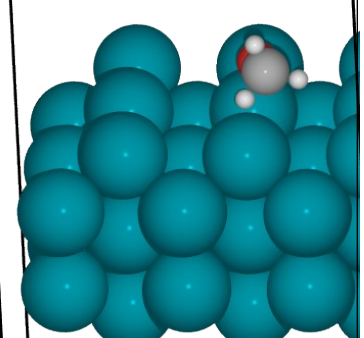
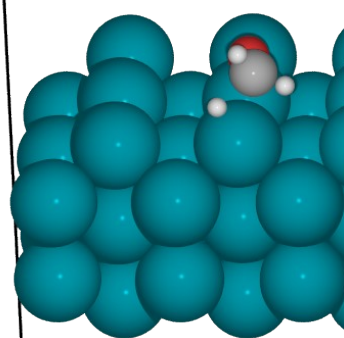
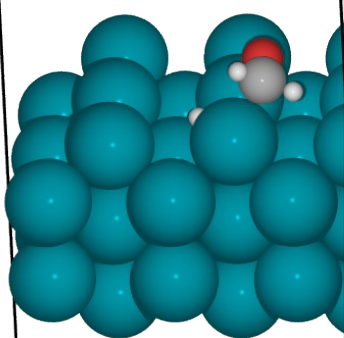
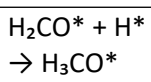
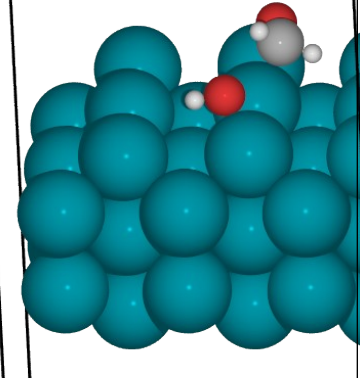
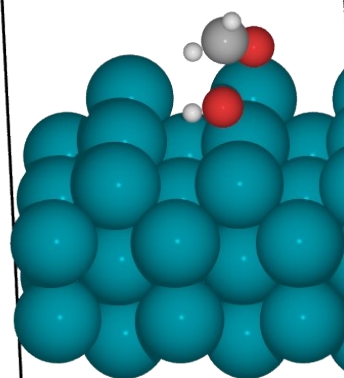
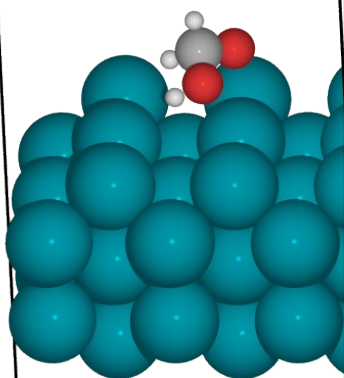
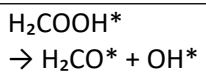
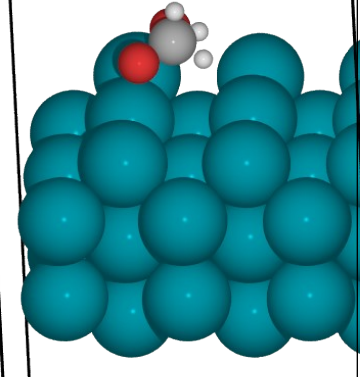
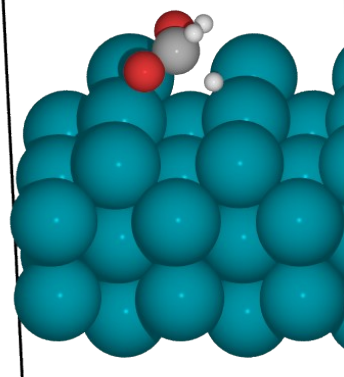
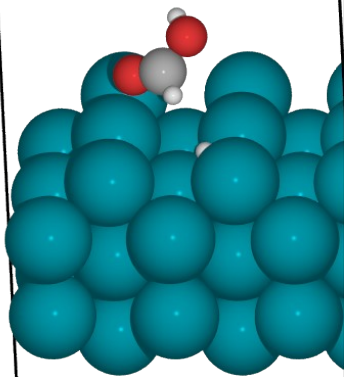
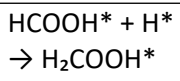
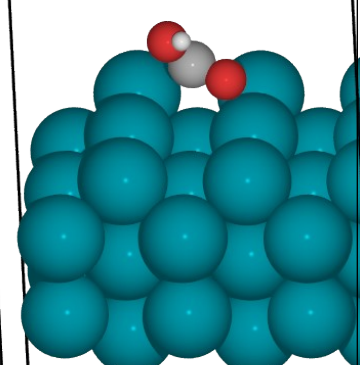
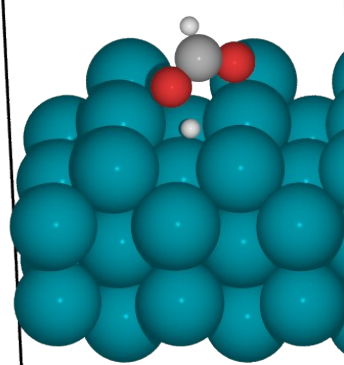
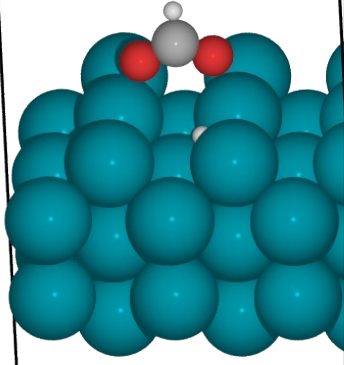
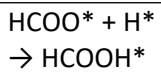
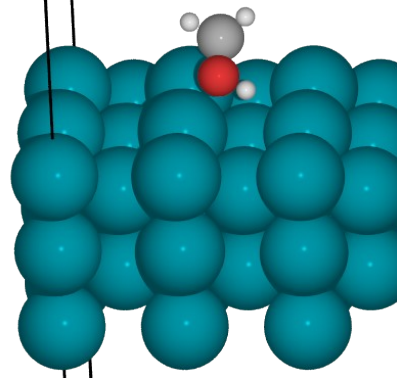
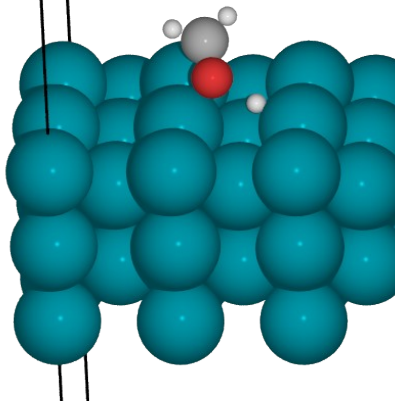
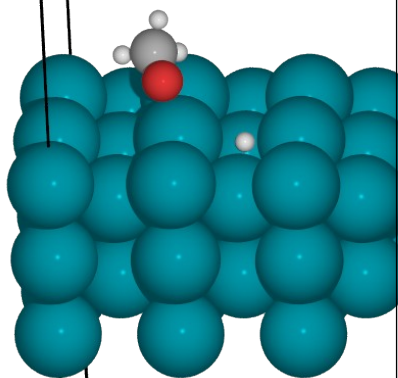
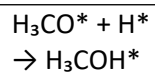


Table S7. Graphical representation of initial, transition state and final geometries in E_{act} calculations on Pd (110) surface. The blue, red, grey and white spheres represent Pd, O, C and H atoms; the black lines indicate the edges of the simulation cell. The full size of the simulation cell, including all unit cell borders, is depicted for the initial reaction step to illustrate the vacuum region size.







S7. Gibbs free energy change diagrams for Pd (100) and (110) surfaces

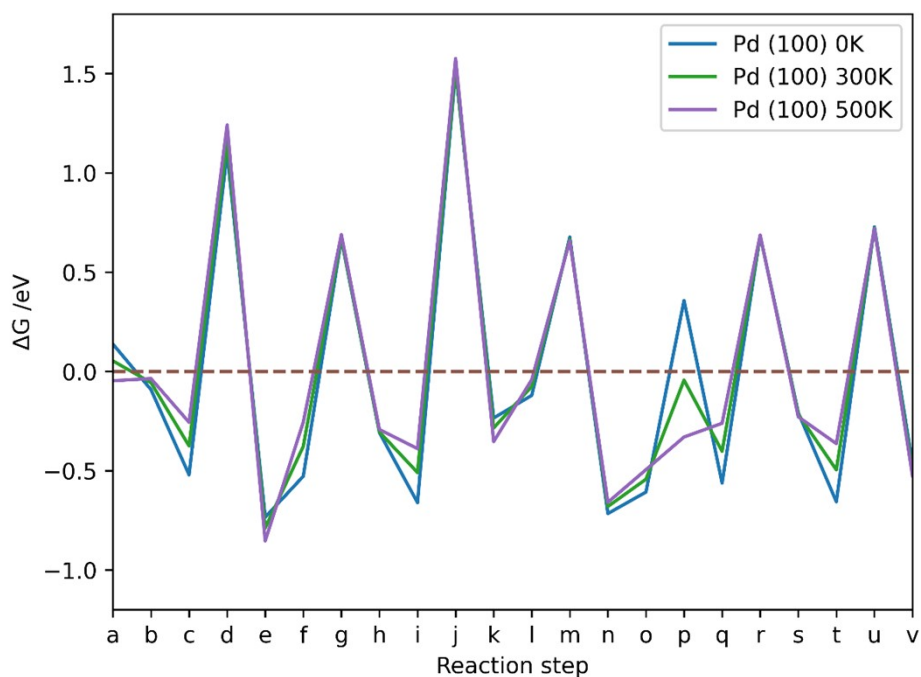


Figure S4. The Gibbs free energy changes between reaction steps in CO₂ hydrogenation reaction via formate on Pd (100) at p of 1 atm and T of 0K, 300K and 500K; reaction steps a-v are explained in Table 5.

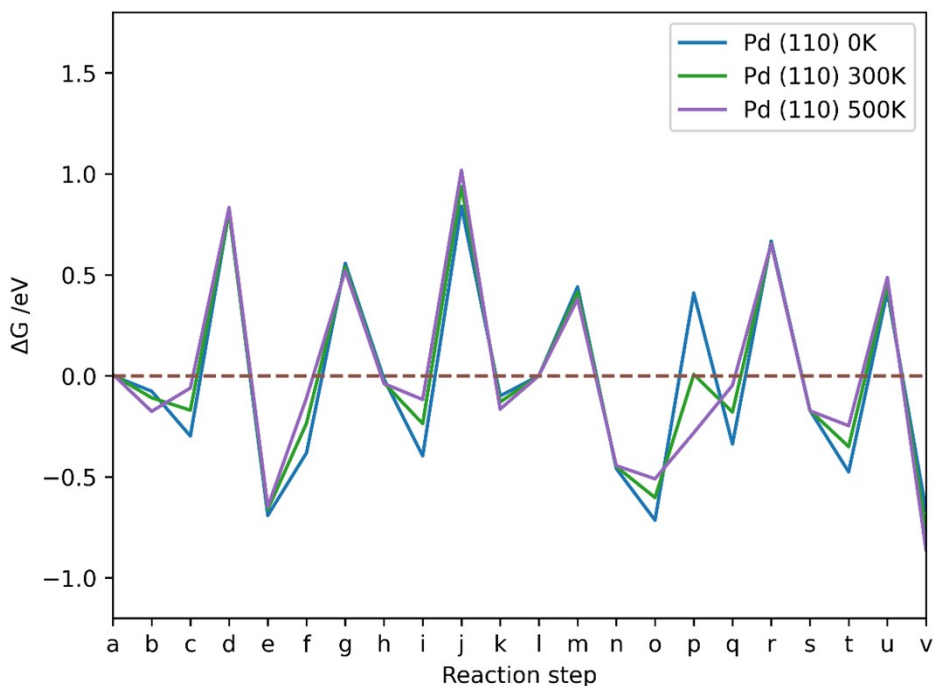


Figure S5. The Gibbs free energy changes between reaction steps in CO₂ hydrogenation reaction via formate on Pd (110) at p of 1 atm and T of 0K, 300K and 500K; reaction steps a-v are explained in Table 5.

References

- (1) Hebbache, M.; Zemzemi, M. Ab Initio Study of High-Pressure Behavior of a Low Compressibility Metal and a Hard Material: Osmium and Diamond. *Phys. Rev. B* **2004**, *70* (22), 224107.
- (2) Arblaster, J. W. Crystallographic Properties of Palladium. *Platinum Metals Rev.* **2012**, *56* (3), 181–189.
- (3) Giri, A. K.; Mitra, G. B. Extrapolated Values of Lattice Constants of Some Cubic Metals at Absolute Zero. *J. Phys. Appl. Phys.* **1985**, *18* (7), L75.
- (4) Borbón, L. O. P. *Computational Studies of Transition Metal Nanoalloys*; Springer Science & Business Media, 2011.
- (5) Massen, C.; Mortimer-Jones, T. V.; Johnston, R. L. Geometries and Segregation Properties of Platinum–Palladium Nanoalloy Clusters. *J. Chem. Soc. Dalton Trans.* **2002**, No. 23, 4375–4388.
- (6) Bucko, T.; Lebègue, S.; Hafner, J.; Ángyán, J. Tkatchenko-Scheffler van Der Waals Correction Method with and without Self-Consistent Screening Applied to Solids. *Phys. Rev. B* **2013**, *87*.
- (7) Tkatchenko, A.; DiStasio, R. A.; Car, R.; Scheffler, M. Accurate and Efficient Method for Many-Body van Der Waals Interactions. *Phys. Rev. Lett.* **2012**, *108* (23), 236402.
- (8) Tkatchenko, A.; Ambrosetti, A.; DiStasio, R. A. Interatomic Methods for the Dispersion Energy Derived from the Adiabatic Connection Fluctuation-Dissipation Theorem. *J. Chem. Phys.* **2013**, *138* (7), 074106.